Atmos. Chem. Phys., 25, 13475–13491, 2025 https://doi.org/10.5194/acp-25-13475-2025 © Author(s) 2025. This work is distributed under the Creative Commons Attribution 4.0 License.





Potential contribution to secondary aerosols from benzothiazoles in the atmospheric aqueous phase based on oxidation and oligomerization mechanisms

Qun Zhang^{1,2}, Wei Zhou¹, Shanshan Tang⁴, Kai Huang¹, Jie Fu¹, Zechen Yu¹, Yunhe Teng¹, Shuyi Shen¹, Yang Mei¹, Xuezhi Yang¹, Jianjie Fu^{1,2,3}, and Guibin Jiang^{1,2,3}

Correspondence: Jianjie Fu (jjfu@rcees.ac.cn)

Received: 4 March 2025 – Discussion started: 13 March 2025 Revised: 28 May 2025 – Accepted: 14 June 2025 – Published: 23 October 2025

Abstract. Benzothiazoles (BTs), widely used as vulcanization accelerators in the rubber industry, have frequently been identified in the atmosphere, especially in areas with heavy traffic. BTs can undergo gas-phase oxidation in the atmosphere, which contributes to secondary aerosol mass. However, given their certain water solubility, the atmospheric fate of BTs associated with aqueous-phase transformations is unclear. In this study, the reactions of benzothiazole (BT), 2-methylbenzothiazole (MBT), and 2-chlorobenzothiazole (CBT) with hydroxyl radicals (OH) were investigated. The rate constants of BT, MBT, and CBT reacted with OH radicals were determined to be (8.0 ± 1.8) , (7.6 ± 1.7) , and $(7.6 \pm 1.9) \times 10^9 \,\mathrm{M}^{-1} \,\mathrm{s}^{-1}$ at initial pH2 and (9.7 ± 2.7) , (9.8 ± 2.7) , and $(9.4 \pm 2.7) \times 10^9 \,\mathrm{M}^{-1} \,\mathrm{s}^{-1}$ at initial pH 10, respectively. Lifetimes ranging from several minutes to several hours were estimated under mean OH concentrations in various atmospheric aqueous phases, which are significantly shorter than those estimated under mean OH concentrations in the gas phase. The nanoparticle tracing analysis (NTA) directly shows the formation of nanoparticles from the aqueous-phase photooxidation of the selected BTs. Data analysis of liquid chromatography Orbitrap mass spectrometry (LC-Orbitrap MS) identifies many multifunctional oligomers. Changes in optical property support the formation of oligomers and suggest that the products have the potential to contribute to the atmospheric brown carbon. In addition, higher yields of sulfate are formed after the reactions. It is highlighted that the aqueous-phase oxidation of BTs can contribute to the secondary aerosol mass in the ambient atmosphere, particularly in polluted regions where concentrations of BTs are comparable to those of benzenes, potentially altering the chemical composition and optical properties of atmospheric particles.

1 Introduction

Benzothiazoles (BTs) are a class of aromatic heterocyclic organic compounds with a thiazole ring fused to a benzene ring. BTs are categorized as high-production-volume chemicals, with a reasonable annual global production estimate of hundreds of thousands of tons (Liao et al., 2018). They are used in a variety of industrial and consumer products, mainly including vulcanization accelerators in rubber production, ultraviolet light stabilizers in textiles and plastics, and precursors in the production of pharmaceuticals (Avagyan et al., 2015; Reddy and Quinn, 1997). BTs can also be biogenically produced from plants and microorganisms (De Wever and Verachtert, 1997; Chhalodia et al., 2021; Stierle et al., 1991). The high production, extensive use, and decentralized presence of BTs have resulted in their widespread release into the environment by volatilization, leaching, and abrasion (Luongo et al., 2016; Parker-Jurd et al., 2021; Zhang et al., 2018a; Schneider et al., 2020; Tang et al., 2022a; Bayati et al., 2021; Armada et al., 2022). Moreover, BTs have been commonly detected in human blood, urine, adipose tissue, breast milk, and even amniotic fluid (Liao et al., 2018; Garcia-Gomez et al., 2015; Li et al., 2022; Ferrario et al., 1985; Zhou et al., 2020). BTs have the potential to disrupt the endocrine system, and their exposure in the body may pose a certain risk to human health (Chen et al., 2020; Cao et al., 2023; Zhou et al., 2020; Li et al., 2022). The German Environmental Protection Agency has classified BTs as potentially persistent, mobile, and toxic substances, making them highly concerning (Neumann and Schliebner, 2019).

Commonly used BTs have been detected in the atmosphere of cities worldwide, with concentrations of ΣBTs ranging from tens of pg m⁻³ to several µg m⁻³ (Zhang et al., 2025; Johannessen et al., 2022; Chang et al., 2021; Wu et al., 2021; Nuñez et al., 2020; Dörter et al., 2020; Wei et al., 2025). The mean concentration of Σ_4BTs in 18 major cities worldwide is 66 pg m⁻³, higher than the four types of flame retardants Σ₉PBDEs (polybrominated diphenyl ethers), $\Sigma_{11}NFRs$ (novel flame retardants), HBCDD (hexabromocyclododecane), and TBBPA (tetrabromobisphenol A) with mean values of 42, 42, 15, and 17 pg m⁻³, respectively (Johannessen et al., 2022; Saini et al., 2020). The median concentration of $\Sigma_6 BTs$ in PM_{2.5} in typical cities of China ranges from 305 to 564 pg m⁻³, significantly higher than another widely concerned rubber additive Σ_6 PPDs (p-phenylenediamine antioxidants, with median concentrations of $27-103 \text{ pg m}^{-3}$) (Liao et al., 2021; Zhang et al., 2022). Benzothiazole has the highest content amongst all species of BTs in the atmosphere, whose concentration in the gas phase can reach 3.86 µg m⁻³ in some region, larger than or equivalent to the common anthropogenic species, such as benzene, toluene, xylenes, and benzaldehyde (Dörter et al., 2020). The highest concentration of PM_{2.5}bound BTs can also reach a level of several ng m⁻³ (Liao et al., 2021; Zhang et al., 2020b; Dörter et al., 2020). In addition, BT is also present in urban rain, with a concentration as high as $70 \,\mathrm{ng} \,\mathrm{L}^{-1}$ (Ferrey et al., 2018).

Owing to their extensive use and widespread presence in the atmosphere, the environmental fate of BTs associated with atmospheric transformations has begun to be brought into focus in recent years. The gas-phase oxidation of benzothiazole by OH radicals has been experimentally and theoretically investigated, in which the rate constant has been determined to be $(2.1 \pm 0.1) \times 10^{-12} \, \text{cm}^3 \, \text{molec.}^{-1} \, \text{s}^{-1}$, and the mechanism for the reaction of OH with benzothiazole via the initial attack on different carbon sites has been proposed (Karimova et al., 2024). Simulation experiments of the gas-phase benzothiazole photooxidation with OH radicals indicated that benzothiazole could contribute to secondary organic aerosols after their oxidation into C3-8 organic compounds and could also lead to the production of sulfuric acid (Franklin et al., 2021). Aqueous phases are also significant reaction media in the ambient atmosphere, including clouds, fogs, or wet aerosol particles (Blando and Turpin, 2000; Herrmann et al., 2015; Ervens, 2015; McNeill, 2015). OH radicals are both highly reactive and nonselective in the atmospheric aqueous phase compared to other atmospheric oxidants, which can significantly shorten the atmospheric lifetime of pollutants (Herrmann, 2003). Based on laboratory, modeling, and field studies conducted over the past decades, there has been increasing evidence that aqueousphase processing affects the formation of both organic and inorganic components of secondary aerosols and contributes to the production of light-absorbing matter, which has the potential to influence climate (Lv et al., 2025; Mei et al., 2025; Li et al., 2023b; Zhang et al., 2018b, 2020a; Ervens, 2015; Herrmann et al., 2015; Laskin et al., 2015; McNeill, 2015; Meagher et al., 1990). BTs are water-soluble, as the water solubility of benzothiazole is experimentally determined to be $4300 \,\mathrm{mg} \,\mathrm{L}^{-1}$ at $25 \,^{\circ}\mathrm{C}$ (Wishart et al., 2022). It is higher than or comparable to many compounds emitted from biomass burning that have been proven to undergo aqueousphase processes and contribute to secondary organic aerosols in the atmosphere, such as syringic acid $(1548 \,\mathrm{mg}\,\mathrm{L}^{-1})$ at 25 °C), α -terpineol (710 mg L⁻¹ at 25 °C), and vanillic acid $(2791 \text{ mg L}^{-1} \text{ at } 25 \,^{\circ}\text{C})$ (Li et al., 2021, 2020; USEPA, 2012; Tang et al., 2020b). Therefore, understanding the photooxidation reactions of BTs in the aqueous phase is significant, not only for the integrated determination of the atmospheric fate of BTs but also for assessing their potential contributions to both organic and inorganic components of secondary aerosols due to their nature as sulfur-containing organic compounds. However, the detailed aqueous-phase oxidation mechanisms of BTs in the atmosphere remain largely unexplored, hindering a holistic understanding of their atmospheric chemistry and potential health risks.

The objective of this study is to investigate the aqueousphase transformation of BTs by OH radicals in the atmosphere. Therefore, photooxidation reactions of OH radicals and frequently detected BTs in the atmosphere, such as benzothiazole (BT), 2-methylbenzothiazole (MBT), and 2-chlorobenzothiazole (CBT) (Fig. 1) (Liao et al., 2021; Nuñez et al., 2020; Dörter et al., 2020), were carried out at room temperature in an aqueous solution using a photoreactor. Kinetics of reactions of selected BTs and OH radicals are determined. Products from reactions of selected BTs and OH radicals were analyzed, based on which the reaction mechanisms were proposed.

2 Materials and methods

2.1 Chemicals

Benzothiazole (BT, > 96.0%), 2-methylbenzothiazole (MBT, > 98.0%), 2-chlorobenzothiazole (CBT, > 98.0%), p-toluic acid (TA, > 98.0%), L-phenylalanine (LPA, > 98.0%), and sodium hydroxide (NaOH, $1 \, \text{mol} \, \text{L}^{-1}$ in water) were purchased from Tokyo Chemical Industry (Japan). Suberic acid (SA, $\geq 99\%$) was purchased from Adamas (Swiss). Perchloric acid (HClO₄, $0.1 \, \text{mol} \, \text{L}^{-1}$ in water) was purchased from Aladdin (China). Hydrogen peroxide (H2O₂, $30 \, \text{wt} \, \%$ in water) was purchased from Sinopharm (China). All chemicals were used as received without further purification. Ultrapure water ($18.2 \, \text{M}\Omega \, \text{cm}$ at $25 \, ^{\circ}\text{C}$) was supplied by a Milli-Q water purification system. All solutions were freshly prepared for each experimental run.

2.2 Aqueous-phase photoreactor

Aqueous photochemical experiments were conducted in a 250 mL quartz glass vessel with a path length of 7 cm, and 200 mL of solution was initially used for the reaction. The solution was continuously stirred with a glass magnetic stir bar and irradiated with a UVB lamp (peak emission 306 nm, 6 W, G6T5E, Sankyo-Denki, Japan), whose wavelength falls into the typical actinic region (> 290 nm) of the solar spectrum for generation of OH radicals through $\rm H_2O_2$ photolysis to trigger oxidation reactions. All experiments were carried out at 298 \pm 1 K.

2.3 Kinetic experiments

A relative rate technique is widely used for the investigation of aqueous-phase kinetics as it does not involve the concentration of OH radicals, and the reactant concentration does not need to be accurately known (Aljawhary et al., 2016). Therefore, the relative rate method was used to determine the second-order rate constants of the reaction of BT, MBT, and CBT (denoted as BTs) with OH radicals in this study. This method relies on the assumption that BTs and the reference compounds are removed solely by reacting with OH radicals. The rate constant was obtained by detecting the relative losses of BTs and the reference compounds with well-known rate constants of reactions with OH radicals. The rate

Table 1. Second-order rate constants for the aqueous-phase oxidation of reference compounds by OH radicals (Buxton et al., 1988).

| Reference compounds | | k for oxidation by OH $(M^{-1} s^{-1}) \times 10^9$ | | | |
|---------------------|---------------|---|--|--|--|
| | pH = 2 | pH = 10 | | | |
| Suberic acid | 4.8 ± 0.4 | _ | | | |
| L-Phenylalanine | 5.7 ± 0.5 | 9.0 ± 0.9 | | | |
| p-Toluic acid | _ | 8.0 ± 0.8 | | | |

constant was calculated by Eq. (1).

$$\ln \frac{[\text{BTs}]_0}{[\text{BTs}]_t} = \frac{k_{\text{BTs}}}{k_{\text{Ref}}} \ln \frac{[\text{Ref}]_0}{[\text{Ref}]_t} \tag{1}$$

In Eq. (1), $[BTs]_0$ and $[BTs]_t$ are the concentrations of BTs at time zero and time t; $[Ref]_0$ and $[Ref]_t$ are the concentrations of reference compounds at time zero and time t; and k_{BTs} and k_{Ref} are second-order rate constants $(M^{-1}s^{-1})$ for reactions of OH radicals and compounds of interest and reference, respectively.

In the real atmosphere, the range of pH values in the aqueous phase is from highly acidic to slightly alkaline in both dilute cloud droplets and concentrated deliquescent particles (Herrmann et al., 2015). Therefore, initial pH 2 and 10 were chosen to simulate the aqueous phase in the atmosphere for kinetic studies. In experiments for rate constants determination, the reaction mixture was a 1-2 µM aqueous solution of a kind of BTs with a total volume of 100 mL. The initial pH of the reaction solution was adjusted to 2 or 10 with HClO₄ or NaOH, which was measured by a pH meter (SevenCompact, Mettler Toledo). 1 mM of H₂O₂ in the reaction mixture was photolyzed with UVB irradiation to generate OH radicals. Two reference compounds were used under each pH condition, of which rate constants are listed in Table 1 (Buxton et al., 1988). Kinetic experiments were performed in triplicate at initial pH 2 and 10, with the concentration ratio of BTs to the reference compounds adjusted to ensure accurate determination of the rate constants for the reactions of BTs with OH radicals.

The uncertainty of the determined rate constant of BTs reacted with OH radicals was derived from the uncertainty of the linear fit of the plot of $\ln([BTs]_0/[BTs]_t)$ versus $\ln([Ref]_0/[Ref]_t)$ and the error of the rate constant of the reference compound (Kramp and Paulson, 1998). The uncertainty of the slope was twice the standard error (Tang et al., 2020b; Li et al., 2021). It was mainly attributed to the analytical instrument for determination of relative losses of BTs and reference compounds (Messaadia et al., 2013). Uncertainties of reference compounds were estimated at 10 % according to a previous study (Buxton et al., 1988).

During a kinetic experiment, 1 mL aliquots were sampled from the reaction beaker at designated time intervals, in which a total of 10 mL solution was removed from the

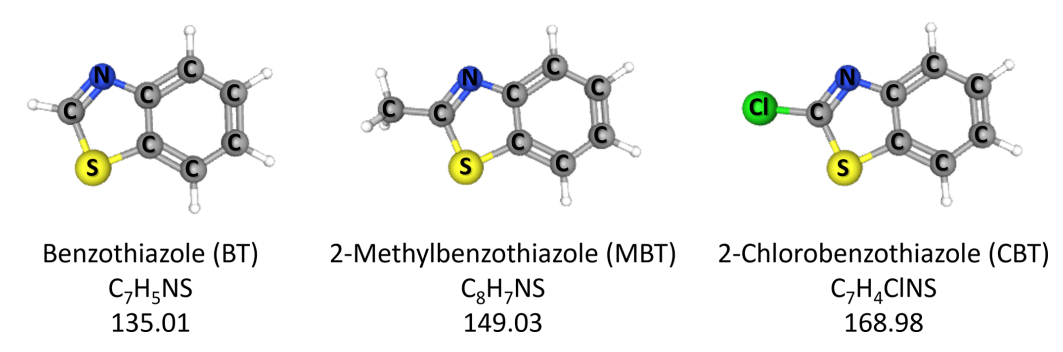


Figure 1. Structures, formula, and molecular weights of benzothiazole (BT), 2-methylbenzothiazole (MBT), and 2-chlorobenzothiazole (CBT) (white balls represent H atoms).

100 mL solution with a negligible effect on the determination of kinetics. Relative losses of BTs and reference compounds were immediately detected with a liquid chromatograph (LC, Vanquish, Thermo Scientific, USA) coupled with a triple-quadrupole mass spectrometer (MS, TSQ Altis Plus, Thermo Scientific, USA) equipped with an electrospray ionization (ESI) source. The multiple reaction monitoring (MRM) mode was used in the MS operation, and the full description of the LC-MS analysis method has been provided in the Supplement (Sect. S1). Control experiments were conducted to demonstrate that the degradation of BTs was only attributed to their oxidation by OH radicals. Experiments without UVB illumination were to ensure that H2O2 would not degrade BTs, and photodegradation experiments without the addition of H2O2 were to determine if BTs would undergo direct photolysis. Results of control experiments confirmed that the decay of BTs did not occur during the period of kinetic experiments (Fig. S1 in the Supplement).

2.4 Experiments for product formation

In experiments for product formation, pH 2 and 10 were also chosen to simulate the aqueous phase in the atmosphere. The reaction solution consisted of a kind of BTs ($\sim 0.45 \,\mathrm{mM}$), H₂O₂ (10 mM), and initial pH adjuster (HClO₄ or NaOH) with a total volume of 200 mL. During an experiment, 10 mL aliquots were sampled from the reaction beaker at time intervals of 1 h for subsequent analysis. Concentrations of BTs were obtained with LC-MS, whose method is described in the Supplement (Sect. S1). The experiments were performed for 5 h. The steady-state concentration of OH radicals can be estimated through dividing the loss of BTs by the bimolecular rate constant of BTs with OH radicals (Eq. 2; George et al., 2015). Considering the different parent compounds and the rate constants at pH2 and 10, the steady-state concentration of OH radicals was estimated to be approximately $10^{-14} \,\mathrm{M}.$

$$[OH] = \frac{k'}{k_{BTs+OH}}$$
 (2)

2.5 Measurements of optical properties

Ultraviolet–visible (UV–vis) absorption spectra of the samples collected at time intervals of 1 h were obtained by a UV–vis spectrophotometer (UV-2700i, Shimadzu, Japan) in the range of 200–800 nm with a step size of 1 nm. The sample for UV–vis spectrum measurement was contained in a quartz cuvette with an optical length of 10 mm. Ultrapure water was measured to obtain the baseline as the background spectrum. The total organic carbon (TOC) concentrations were measured on a TOC analyzer (TOC-L-CPH, Shimadzu, Japan) by high-temperature catalytic oxidation. The light-absorbing properties were quantified via the calculation of the mass absorption efficiency at 365 nm (MAE₃₆₅, m² g⁻¹ C) and through Eq. (3) (You et al., 2020; Tang et al., 2022b).

$$MAE_{\lambda} = \frac{A_{\lambda} \times \ln(10)}{C_{\text{mass}} \times l}$$
 (3)

In Eq. (3), A_{λ} is the UV–vis absorbances, C_{mass} is the TOC concentration measured in g m⁻³, and l is the path length (0.01 m).

The fluorescence excitation–emission matrix (EEM) of the samples collected at the initial time (t = 0) and the end time (t = 5 h) of photooxidation reactions was obtained by a fluorescence spectrophotometer (F-4700, Hitachi, Japan) in the three-dimensional scan mode at room temperature. The instrument conditions were set as the following parameters: excitation and emission wavelength ranges were 200–600 and 220–700 nm; scanning intervals were 5 and 2 nm; slit widths were 10 nm; and scan speeds were 30 000 nm min⁻¹. The fluorescence data are calibrated by a previous study prior to analysis of results. It includes instrumental bias correction, inner filter effect correction, removal of Raman and Rayleigh scattering, and blank subtraction (Murphy et al., 2013).

2.6 Measurements of chemical composition of products

Inorganic products of the samples collected at time intervals of 1 h were quantified via ion chromatography (IC, Dionex ICS-6000, Thermo Scientific, USA) using an anion column

(Dionex IonPacTM AS15, 4 mm ID \times 250 mm, Thermo Scientific, USA) with 38 mM KOH as an eluent at a flow rate of 1.2 mL min⁻¹. The sample was filtered through a microporous membrane syringe filter (PTFE, pore size: 0.22 μ m) before the IC measurement.

Organic products of the samples collected at the end time (t = 5 h) of photooxidation reactions were carried out with LC (Vanquish, Thermo Scientific, USA) coupled with the Orbitrap mass spectrometer (Orbitrap Exploris 480, Thermo Scientific, USA) equipped with the ESI probe, and the full description of the LC-Orbitrap MS method has been provided in the Supplement (Sect. S2). The Xcalibur software and Compound Discoverer 3.3 software (Thermo Fisher Scientific Inc., USA) were used to analyze the data from Orbitrap MS. Nanoparticle tracking analysis (NTA, Nanosight NS300, Malvern Panalytical, UK) was used for determination of the number concentration and size distribution profile of nanoparticles in the samples collected at time intervals of 1 h.

3 Results and discussion

3.1 Rate constants for reactions of BTs with OH radicals

Rate constants of BT, MBT, and CBT reacted with OH radicals were obtained at initial pH2 and 10 via the relative rate method. The slope of the fitted straight line obtained by plotting $ln([BTs]_0/[BTs]_t)$ versus $ln([Ref]_0/[Ref]_t)$ is equal to $k_{\rm BTs}/k_{\rm Ref}$. In Fig. 2, the relative kinetic plots obtained were linear ($R^2 > 0.99$), and their intercepts were very close to zero, which demonstrates negligible contribution of secondary reactions (Wang et al., 2015). The fitted slopes in Fig. 1 were used to calculate the rate constants by multiplying the slopes by rate constants of reference compounds. The determined second-order rate constants of BT, MBT, and CBT reacted with OH radicals are listed in Table 2. The rate constants of BT + OH, MBT + OH, and CBT + OH reactions were determined to be (8.0 ± 1.8) , (7.6 ± 1.7) , and $(7.6 \pm 1.9) \times 10^9 \,\mathrm{M}^{-1} \,\mathrm{s}^{-1}$ at initial pH 2 and (9.7 ± 2.7) , (9.8 ± 2.7) , and $(9.4 \pm 2.7) \times 10^9 \,\mathrm{M}^{-1} \,\mathrm{s}^{-1}$ at initial pH 10. The rate constants of selected BTs reacted with OH radicals under the highly acidic condition were slightly lower than those under the weakly alkaline condition. The values of BT, MBT, and CBT were very close under each initial pH condition. The rate constants for the BTs determined in this study are typical of aromatic contaminants (Li et al., 2023b). The second-order rate constant of BT reacted with OH radicals were reported previously, which was determined to be $(8.61 \pm 0.23) \times 10^9 \,\mathrm{M}^{-1} \,\mathrm{s}^{-1}$ at pH 7 and room temperature and consistent with the value in this study (Bahnmüller et al., 2015). However, some previous studies reported lower rate constants of the BT + OH reaction in the aqueous phase, which were 9.5×10^{8} and $3.85 \times 10^{9} \,\mathrm{M}^{-1} \,\mathrm{s}^{-1}$ at pH 7 (Borowska et al., 2016; Andreozzi et al., 2001). The lower values from previous studies are potentially due to the dif-

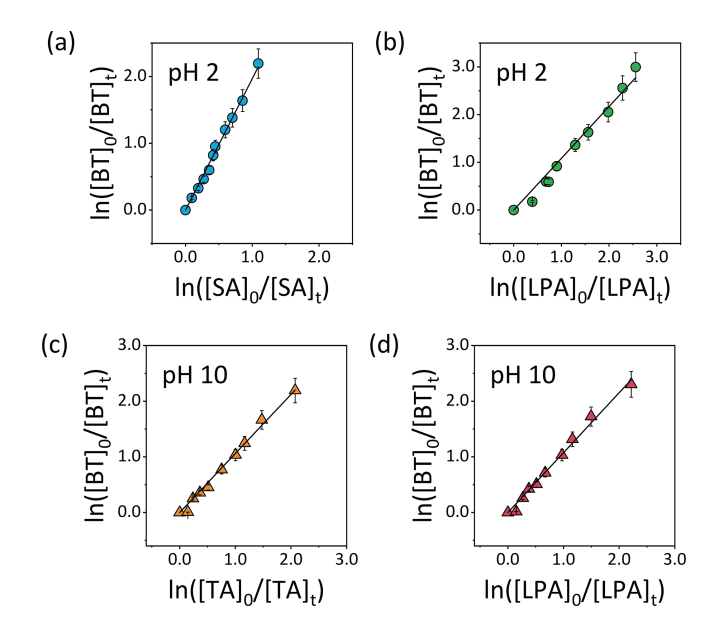


Figure 2. Relative kinetic plots for oxidation of BT with OH radicals in the aqueous phase at initial pH 2 and 10 using SA, LPA, and TA as the reference compounds ($[BTs]_0$: $[Refs]_0 = 1:1$).

Table 2. Kinetics data for BT, MBT, and CBT + OH reactions.

| Reactant | pН | Reference | Number of runs | $(\times 10^9 \mathrm{M}^{-1} \mathrm{s}^{-1})$ |
|----------|----|-----------|-------------------|---|
| BT | 2 | SA | 3 | 8.0 ± 1.8 |
| | | LPA | 3 | |
| | 10 | TA | 3 | 9.7 ± 2.7 |
| | | LPA | 3 | |
| MBT | 2 | SA | 3 | 7.6 ± 1.7 |
| | | LPA | 3 | |
| | 10 | TA | 3 | 9.8 ± 2.7 |
| | | LPA | 3 | |
| CBT | 2 | SA | 3 | 7.6 ± 1.9 |
| | | LPA | 3 | |
| | 10 | TA | 3 | 9.4 ± 2.7 |
| | | LPA | 3 | |

ferences in experimental conditions. The reaction temperatures in the previous studies were 293 K, lower than that in our study. In addition, the material of vessel employed in the previous studies is ordinary glass, but it is quartz glass in our study. The reduction in UV light caused by ordinary glass, together with the higher initial concentration of BT, limits the availability of OH radicals. These factors thus potentially yield lower measured rate constants. Overall, the aqueous-phase kinetic result indicates a high reactivity of BTs with OH radicals, suggesting that atmospheric aqueous-phase oxidation could be a significantly effective process to degrade these contaminants from the air.

3.2 Optical properties

The aqueous-phase reactions of BT, MBT, and CBT with OH radicals were accompanied by the alteration in the optical properties of the reaction solution. It can be directly observed that the color of the reaction solution gradually changed from transparent to yellowish-brown after 5h of UV irradiation (Fig. 3a), which indicated the formation of light-absorbing species from the oxidation process of selected BTs initiated by OH radicals in the aqueous phase. It was consistent with the aqueous-phase oxidation of phenolic compounds in the atmosphere, which have been proven to contribute to the formation of atmospheric brown carbon (Desyaterik et al., 2013; Li et al., 2023b; Teich et al., 2017). The UV-vis absorption spectra of reaction solutions consisting of 0.45 mM BTs and 10 mM H₂O₂ were recorded. In Figs. 3b and S3, the principal absorbance band centered closely as the starting compound and the initial pH differed, which was in the range of 251-256 nm. The principal absorbance band underwent a rapid decrease as the reaction processed. The absorbance bands at 251–256 nm agreed with the characteristic peak of BTs. It was ascribed to the π - π * electronic transitions (> 180 nm) in aromatic compounds (Yi et al., 2018; Santos et al., 2016). Simultaneously, the absorption spectra obviously increased in the range from near-UV (320-400 nm) to vis regions, in which the selected BTs did not absorb light. The increase in spectra in this region suggested the formation of oligomers with large and conjugated π -electron structures (Chang and Thompson, 2010). It could be proposed that aqueous-phase oxidation of BTs initiated by OH radicals led to the degradation of precursor compounds and the formation of oligomeric products. Moreover, it was noted that this process formed products characterized by efficient absorption spectra that smoothly increased from the vis to UV wavelengths, which could contribute to the mass of the atmospheric brown carbon (Laskin et al., 2015).

The UV-vis absorption spectra were converted into mass absorption efficiency (MAE) using Eq. (3). After 5h of photooxidation, the mass absorption efficiency at 365 nm (MAE₃₆₅) values of the light-absorbing substances derived from BTs reached 0.76, 0.74, 0.34, 0.50, 0.85, and $1.02 \,\mathrm{m^2\,g^{-1}}$ for Exps. BT-pH2, BT-pH10, MBT-pH2, MBTpH10, CBT-pH2, and CBT-pH10, respectively (Figs. 3c and S4). Among them, the products from CBT exhibit the highest MAE₃₆₅, resulting from the higher electronegativity of the -Cl group in CBT. MAE₃₆₅ values of the products driven by selected BTs are comparable to those reported for laboratory-generated brown carbon formed via Maillard-like aqueous-phase reactions from carbonyl compounds mixed with ammonium sulfate or amine, where MAE₃₆₅ ranged from 0.15 to 4.50 m² g⁻¹ depending on precursor combinations (Tang et al., 2022b). They are also within the MAE₃₆₅ range observed in ambient brown carbon samples from biomass and coal combustion sources, which span 0.21 to $3.10 \,\mathrm{m}^2\,\mathrm{g}^{-1}$ (Zhang et al., 2024). This suggests that aqueous-phase oxidation of BTs can form lightabsorbing organic products with optical properties relevant to atmospheric brown carbon.

Fluorescence has been used recently to analyze watersoluble organics due to its high sensitivity and nondestructive analysis characteristics. Figures 3d and S5 show the EEM fluorescence spectra before and after 5 h reaction of BT, MBT, and CBT with OH radicals at initial pH 2 and 10. The fluorescence results of reaction systems herein reveal longer emission and excitation wavelengths after 5 h of photooxidation. Red shifts in both emission and excitation wavelengths are usually related to an increase in the size of the ring system and an increase in the degree of conjugation (Chang and Thompson, 2010). This change in the fluorescence spectra also suggests the degradation of the initial compound, and the newly formed compounds at longer wavelengths may have a more complex structure than its precursor, probably with the presence of condensed aromatic ring and other π electron systems, with a high level of conjugation (Chen et al., 2002). Moreover, EEM fluorescence features of products driven by BTs are consistent with the LO-HULIS (lessoxygenated humic-like substances) group, a subclass of atmospheric brown carbon identified in studies of ambient aerosols (Jiang et al., 2022). LO-HULIS are less-oxygenated and nitrogen-containing aromatic compounds commonly observed in biomass burning aerosols. Given the spectral similarity, the aqueous-phase OH oxidation products of BTs in our study can be reasonably classified as LO-HULIS-type chromophores, further indicating a potential for contributing to the light absorption of aerosols.

3.3 Formation of nanoparticles

The reactions of BT, MBT, and CBT with OH radicals at initial pH 2 and 10 in the aqueous phase can lead to the formation of nanoparticles. Figures 3g and S7 show NTA images of samples collected before and after 5 h of photooxidation of BT, MBT, and CBT with OH radicals at initial pH 2 and 10. It can be obviously observed that there are rarely particles in a NTA view from the samples collected before irradiation, but the particles are widely present after 5 h of photooxidation in all reaction solution samples. In Figs. 3f and S8, NTA shows that the particles formed from photooxidation of the selected BTs are in the nanometer scale, with size distributions ranging from 50 to 400 nm. In Figs. 3e and S6, the number concentration of the nanoparticles after 5 h of photooxidation was on the order of 10^8 particles mL⁻¹, much greater than that of nanoparticles before irradiation. The size distribution shows large polydispersity, with individual particles varying in size from a few to several hundred nanometers. While previous studies have reported the formation of oligomeric and polymeric products in atmospheric relevant aqueous-phase reactions (Li et al., 2023a, b; Tang et al., 2022b), direct detection of newly formed nanoparticles remains rare. The observed nanoparticles may originate from

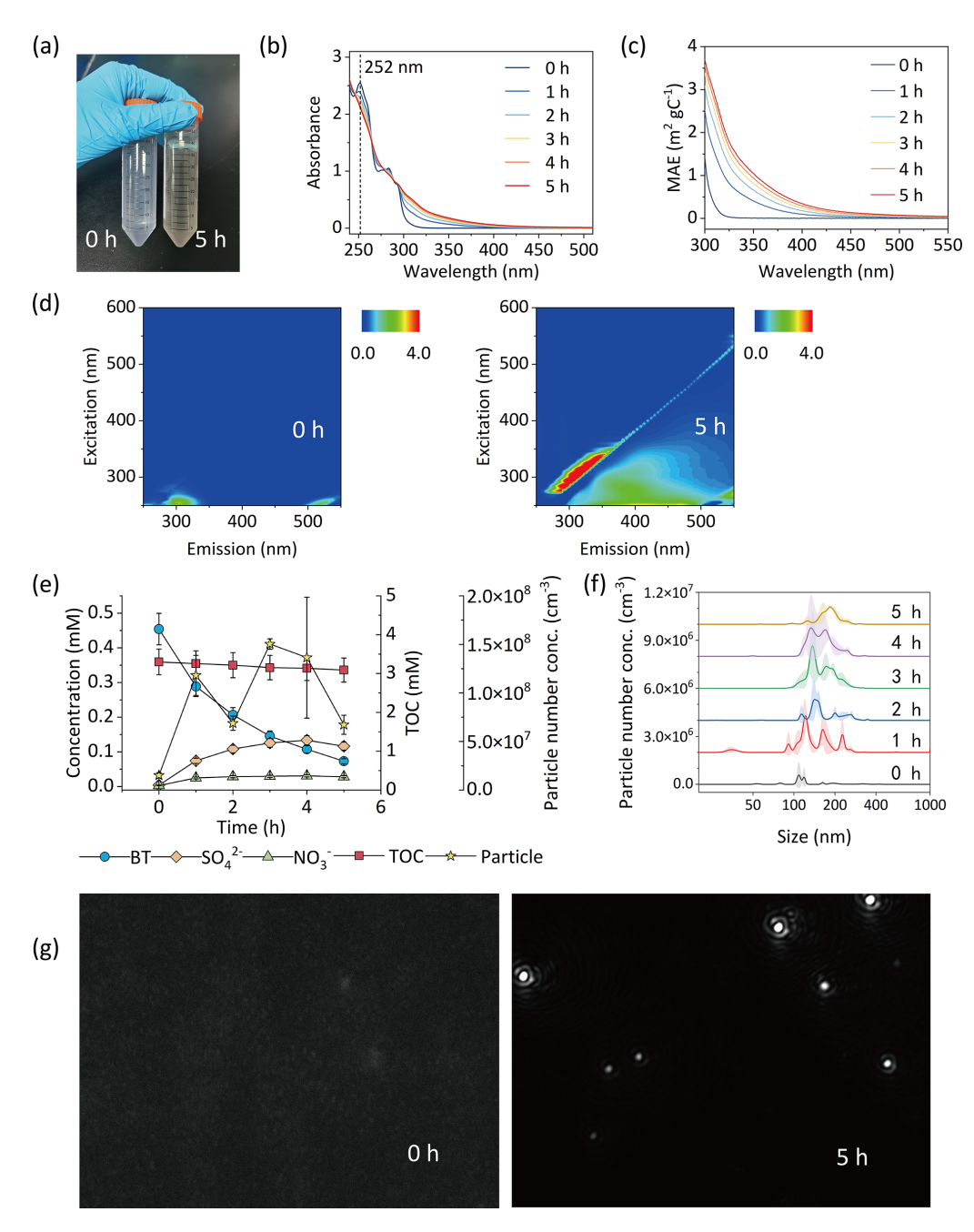


Figure 3. Characterization plots of the reaction solution in Exp. BT-pH2. The change in solution color (a). UV-vis absorption spectra (b) and mass absorption efficiency (MAE) (c) of reaction solution collected at reaction time intervals of 1 h. The change in EEM fluorescence spectra (d). Time profiles of BT degradation, inorganic product formation (SO_4^{2-} , NO_3^{-} , and CI^{-}), particle formation, and total organic carbon (TOC) concentration (e). Size distribution of nanoparticles formed at reaction time intervals of 1 h (f). The change in NTA images (g).

the aggregation of oligomeric products from aqueous-phase oxidation of BTs, highlighting a potentially important but under-recognized route of secondary aerosol formation from aqueous-phase chemistry. It is noteworthy that NTA provides only an approximate estimation of nanoparticles within a particle size range of 10–2000 nm. Additionally, nanoparticles may undergo agglomeration or deagglomeration and may partially dissolve during the transfer from the reaction so-

lution. It can significantly impact particle concentrations and size distributions. Therefore, there should be awareness that the particle size distributions may not be precisely reflected.

3.4 Product analysis and mechanisms

IC measurements were performed for the analysis of inorganic products formed from the photooxidation of BT, MBT,

and CBT with OH radicals in the aqueous phase. In BT and MBT experiments inorganic products contain SO_4^{2-} and NO_3^- , and in CBT experiments they contain SO_4^{2-} , NO_3^- , and Cl⁻. Figure 3e and S6 show that in the photooxidation of selected BTs, inorganic products gradually generate with the degradation of parent compounds. But the formation yields of inorganic products are different regardless of the parent compounds. The molar yields of SO_4^{2-} are in the range of 19.4 %-46.6 %, significantly higher than those of NO₃⁻, which falls within 10.1 % in the experiments of selected BTs (Table S3 in the Supplement). It is worth noting that in the CBT experiments the molar yields of Cl⁻ are the highest among the inorganic products, which are in the range of 61.5 %-87.1 %. The analysis of inorganic products in the reaction solutions indicates that aqueous-phase oxidation of BTs has the capacity to form sulfate in the atmosphere and that nitrate and chloride can be generated from specific BTs. It possibly suggests the presence of inorganic aerosol produced during aqueous-phase oxidation of BTs in the atmosphere. In a previous study, a laboratory simulation study of gas-phase oxidation of BTs in the atmosphere was conducted using a Potential Aerosol Mass Oxidation Flow Reactor (PAM-OFR). The result indicates that gas-phase oxidation of BTs has the capacity to form sulfur dioxide and sulfuric acid in the atmosphere, possibly suggesting the generation of sulfate aerosol during oxidation of BTs (Franklin et al., 2021). Considering both aqueous- and gas-phase oxidation results, atmospheric oxidation of BTs appears to be a potential source of sulfate aerosols, given the significant sulfate yields observed from the oxidation of sulfur-containing structures.

LC-ESI-Orbitrap MS measurements were performed in both positive- and negative-ion ESI modes for the analysis of organic products formed from the photooxidation of BT, MBT, and CBT with OH radicals in the aqueous phase. The raw data from LC-ESI-Orbitrap MS were processed with deconvolution, aligning retention times, subtraction of background compounds, and composition prediction. The number of atoms (${}^{12}C \le 30$, ${}^{1}H \le 30$, ${}^{16}O \le 20$, ${}^{14}N \le 10$, ${}^{32}S \le 10$, and $^{35}Cl \le 5$) and a constraint of 4 ppm mass tolerance are applied as constraints to obtain the elemental composition. Many organic products with assigned molecular formulas and certain retention times were ultimately identified. Figure 4a shows that organic products formed by each photooxidation experiment of the selected BTs contain hundreds of identified compounds in both ESI modes. This suggests that the aqueous-phase oxidation of BTs has the potential to considerably enhance the diversity of chemical composition in the atmosphere. Meanwhile, products contained more identified compounds in positive-ion (+ESI) mode than in negative-ion (-ESI) mode, which suggests a possible enrichment of basic functionalities in the product mixture, as such groups are generally more amenable to ionization in +ESI mode (Lin et al., 2012). The numbers of identified compounds between +ESI and -ESI modes are less different, and the identified compounds across different carbon atom numbers (nC) in both modes are irregular. This indicates that a combined consideration of +ESI and -ESI modes is necessary for product analysis rather than a single mode. It can also be observed from Fig. 4a that the number of identified compounds shows obviously periodic fluctuation with the nC. Four crest values can be observed from the BT experiments, which are at nC 7, 13–14, 21–22, and 27–28. The nC difference value is in the vicinity of 7, which is the nC of the BT molecular formula. Similar patterns can be observed from MBT and CBT experiments. It suggests the generation of oligomers with the nC of parent compounds as the mainly repetitive units, which probably contribute to the formation of nanoparticles in the aqueous-phase photooxidation reactions of the selected BTs with OH radicals.

The molecular formula of identified compounds can be classified into CHO, CHON, CHOS, and CHONS groups according to their elementary composition (Tang et al., 2020a). CHONS compounds account for the largest proportion of the overall molecular formula of identified compounds, around 90% in +ESI mode and 80% in -ESI mode for BT and MBT oxidation systems (Fig. 4b). In the CBT experiment, CHONS compounds alone account for only 30 %-40 % of the total identified molecular formulas. However, when CHONSCl compounds are included, the combined proportion of CHONS and CHONSCl compounds becomes comparable to the fraction of CHONS compounds identified in the BT and MBT experiments. CHONS compounds have been shown to contribute significantly to particle light absorption, with higher mass absorption efficiencies observed in CHONS-rich fractions (Zhang et al., 2024; Bao et al., 2023). With the formation of abundant CHONS species, the aqueous-phase oxidation of BTs may indicate a potential contribution to the climate-relevant properties of brown carbon through enhanced light absorption. In addition, CHON compounds in the experiments of selected BTs (CHON + CHONCl compounds in CBT experiments) account for $\sim 10\%$ of the overall molecular formula of identified compounds, significantly higher than the CHOS compounds (CHOS + CHOSCl compounds in CBT experiments). It is consistent with the lower molar yields of NO₃⁻ than those of SO₄²⁻ formation in the inorganic product measurements. In CBT experiments the proportion of organic products containing Cl atoms is lower than that of organic products containing S and N atoms, which is consistent with the highest molar yields of Cl⁻. It should be noted that in this study the LC-Orbitrap MS analysis provides more qualitative insights, as quantitative determination was limited and not conducted. It can be considered and developed for further characterization of the formation and evolution of organic products.

The structures of BT and proposed products and pathways in the reaction of BT with OH radicals are shown in Fig. 5. The N, C5, and C7 atoms have relatively lower charge distribution and high electron density, which should be the reac-

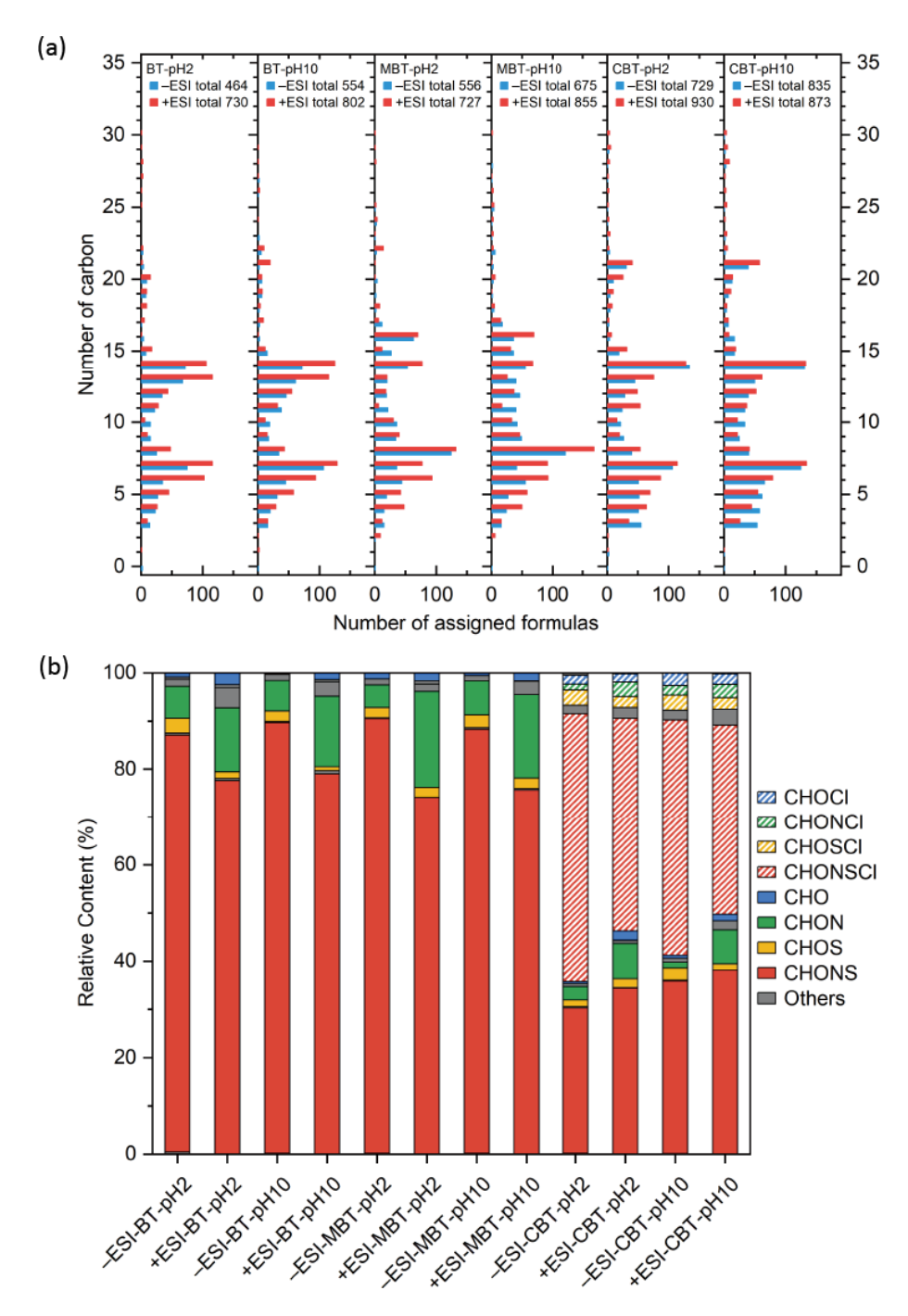


Figure 4. Plots of blank-corrected Orbitrap mass spectra of 5 h of photooxidation of BT, MBT, and CBT with OH radicals at initial pH2 and 10 in negative (-ESI) and positive (+ESI) ion modes. The total number of assigned formulas as a function of the number of carbon atoms (a). The percentages of number distribution of CHO, CHON, CHOS, CHONS, CHOCl, CHONCl, CHONSCl, and other assigned molecular formula (b).

tive sites for electrophilic radical attack (Zhou et al., 2019). OH radicals can electrophilically attack the heterocycle ring or the benzene ring of BT in the first step, leading to the H abstraction and formation of Radicals (I) or (II), respectively (Fig. 5a). Then, the organic radicals would further react with OH radicals, forming hydroxylated BT. It is worth

paying attention to 2-hydroxybenzothiazole (2OBT) formed from Radical (I). Liao et al. (2021) explored six PM_{2.5}-bound BTs in three typical Chinese cities and found that OBT was always predominant, accounting for 50 %–80 % of total BTs. The hydroxylated BT formed from Radical (II) has four isomers featuring a hydroxy group at C4–7 positions. Hydrox-

ylated BTs can be further attacked by OH radicals to form hydroxylated radicals. Tens of dihydroxylated and trihydroxylated BTs can be generated and measured in mass spectra. Zhou et al. (2019) studied the removal of BT in persulfate promoted wet air oxidation (PWAO) and found hydroxylated and dihydroxylated BTs using ultra-performance liquid chromatography quadrupole time-of-flight mass spectrometry (UPLC-QTOF-ESI-MS), but trihydroxylated BTs were not measured. It was proposed that the UV/persulfate degradation of benzothiazole could result in the formation of dihydroxylated and trihydroxylated BTs based on the UPLC-QTOF-ESI-MS, but hydroxylated BTs were not mentioned (Lai et al., 2023). 2OBT tends to undergo heterocyclic ring cleavage by the C2-S bond being broken as this bond has the largest bond length in the molecule that more easily breaks (Fig. 5b) (Zhou et al., 2019). A series of chemical components obtained from mass spectra can verify this reaction pathway. Following the breakage of the heterocyclic ring, a batch of carboxylic acids with a benzene ring are generated step by step, accompanied by the formation of inorganic products, e.g., SO_4^{2-} and NO_3^{-} . This process is along with a decrease in the nC in products. Then, the benzene moiety goes through a ring-opening process, leading to a further decrease in nC. The process of ring opening of thiazole and benzene moieties leads to the formation of products with nC less than the parent compound BT. Figure 5c shows an example of the fragmentation of dihydroxy BTs, which is similar to the fragmentation pathway of 20BT. The benzene moiety of dihydroxy BTs can undergo the carbonylation process, leading to the formation of quinone compounds. The ringopening process takes place, which leads to the formation of dicarboxylic acids and an nC decrease in products.

Moreover, multifunctional oligomers can be generated from the reaction of BT and OH radicals in the aqueous phase. Radical (I) can undergo C-C coupling with one another at the C7 position, resulting in the formation of an isomeric form of the dimer C₁₄H₈NS (Fig. 5d). Additionally, C-C coupling can take place between a Radical (I) and a Radical (II) or between two Radicals (I), leading to the generation of further isomeric forms of the dimer $C_{14}H_8NS$. Then the dimers further react with OH radicals, forming polyhydroxylated dimers C₁₄H₈NSO₁₋₆ (Fig. 5e). BT dimers can react with Radicals (I) or (II) to form BT trimers with a batch of isomers. Then polyhydroxylated trimers can be generated. It should be noted that Fig. 5 only illustrates some examples of the reaction pathways between BT and OH radicals for the purpose of providing clear descriptions. As a matter of fact, processes of hydroxylation, carbonylation, fragmentation, oligomerization, and ring-opening have combined effects in the reaction system, ultimately leading to the formation of hundreds of multifunctional products with a large range of nC from a parent compound. It is reasonable to speculate that multifunctional oligomers may contribute to the formation of nanoparticles from aqueous-phase oxidation of BT by OH radicals.

4 Conclusions

The atmospheric aqueous-phase lifetime (τ) of BT, MBT, and CBT initiated by OH radicals can be evaluated by Eq. (4).

$$\tau = 1/(k_{\rm BTs} \times [\rm OH]) \tag{4}$$

In Eq. (4), $k_{\rm BTs}$ is the rate constants of BT, MBT, and CBT reacted with OH radicals determined in this study, and [OH] represents the concentration of OH radicals in the atmosphere under various aqueous-phase conditions (Bianco et al., 2020; Arakaki et al., 2013; Herrmann et al., 2010). The aqueous-phase OH concentrations and the evaluated lifetimes of BT, MBT, and CBT are summarized in Table 3. Atmospheric aqueous phases are generally categorized into cloud droplets and deliquescent particles and can be further classified by location as urban, remote, and maritime regions. Previous studies give the mean value of OH concentrations in various aqueous phases (Bianco et al., 2020; Herrmann et al., 2010). The atmospheric lifetimes determined for BT, MBT, and CBT are in the range from 0.01 to 0.4 h in deliquescent particles and 0.01 to 10.4 h in cloud particles. Previous studies also model varying ranges of OH concentrations in each aqueous phase, from 10² to 10⁴ fold (Bianco et al., 2020; Arakaki et al., 2013; Hermann et al., 2010). For example, the OH concentrations are from 10^{-14} to 10^{-12} M in remote deliquescent particles and 10^{-16} to 10^{-12} M in urban deliquescent particles. The 10²- to 10⁴-fold ranges in aqueous-phase OH concentrations produce 10²- to 10⁴-fold spread in estimated lifetimes of BTs based on Eq. (4). The large range of OH concentrations leads to large uncertainties of estimated lifetimes of BTs. In urban regions, the OH concentrations are modeled to be from 10^{-16} to 10^{-12} M in both cloud droplets and deliquescent particles, which leads to considerably large ranges of lifetimes of BTs, from several minutes to several days. In addition to this, in most cases, the lifetimes of BTs can be limited to several minutes to several hours. In general, the selected BTs tend to be transformed by aqueous OH radicals, especially in the region of their emission sources, and in rare cases they are also probably more persistent in the aqueous phase. It should be noted that the pH conditions in this study may introduce additional uncertainty into the estimated atmospheric lifetimes of BTs, due to the pH-dependent variability in aqueous-phase OH radical concentrations (Wolke et al., 2005; Herrmann et al., 2005).

The atmospheric gas-phase lifetime of BT, MBT, and CBT initiated by OH radicals can also be evaluated by Eq. (4). Rate constants of BT, MBT, and CBT reacted with OH radicals have been estimated using the Atmospheric Oxidation Program for Microsoft Windows (AOPWIN) model, which are 0.7, 1.8, and 0.5×10^{-11} cm³ molec. $^{-1}$ s⁻¹, respectively (USEPA, 2012). The AOPWIN model is based upon structure–activity relationship (SAR) methods developed by Atkinson and coworkers, which has been widely used to predict the rate constants for atmospheric gas-phase reac-

Figure 5. Proposed reaction mechanism and structures of partial products of BT oxidized by OH radicals in the aqueous phase. Red structures with formulas and molecular weight are the products assigned in Orbitrap mass spectra.

tions between organic molecules and OH radicals (Atkinson and Arey, 2003; Atkinson, 1986). A typical peak OH radical concentration at midday is 10⁷ molec.cm⁻³, and a 24 h average OH radical concentration is 10⁶ molec.cm⁻³ (Prinn et al., 2001; Finlayson-Pitts and Pitts, 2000). Table 3 also summarizes the gas-phase lifetimes of the selected BTs

in the atmosphere, which falls in the range of $1.5-5.6\,\mathrm{h}$ at $1.0\times10^7\,\mathrm{OH\,cm^{-3}}$ and $15-56\,\mathrm{h}$ at $1.0\times10^6\,\mathrm{OH\,cm^{-3}}$. In addition, the rate constant of the BT + OH reaction has been experimentally determined using the relative rate method, which is $(2.1\pm0.1)\times10^{-12}\,\mathrm{cm^3\,molec.^{-1}\,s^{-1}}$ (Karimova et al., 2024). The gas-phase lifetime of BT is translated to be

Table 3. Atmospheric lifetimes of BT, MBT, and CBT initiated by OH radicals in various aqueous and gas phases.

| | Ref. | | [OH] ^a | $	au_{ m BT}$ in ${ m h}^{ m b}$ | | τ _{MBT} in h ^b | | τ_{CBT} in h^b | |
|---------------------------------------|---|--------------------|---|----------------------------------|----------------------|------------------------------------|----------------------|-----------------------|----------------------|
| Urban cloud droplets | Herrmann et al. (2010) and Bianco et al. (2020) | Mean Max Min | 3.5×10^{-15} 1.6×10^{-14} 2.9×10^{-16} | 9.9 2.2 119.7 | 8.2 1.8 98.7 | 10.4 2.3 126.0 | 8.1 1.8 97.7 | 10.4 2.3 126.0 | 8.4 1.8 101.9 |
| | Arakaki et al. (2013) | Max Min | 1.9×10^{-12} 1.0×10^{-14} | 0.02 3.5 | 0.02 2.9 | 0.02 3.7 | 0.01 2.8 | 0.02 | 0.02 3.0 |
| Remote cloud droplets | Herrmann et al. (2010) and Bianco et al. (2020) | Mean Max Min | 2.2×10^{-14} 6.9×10^{-14} 4.8×10^{-15} | 1.6 0.5 7.2 | 1.3 0.4 6.0 | 1.7 0.5 7.6 | 1.3 0.4 5.9 | 1.7 0.5 7.6 | 1.3 0.4 6.2 |
| | Arakaki et al. (2013) | Max Min | $2.4 \times 10^{-12} 2.6 \times 10^{-14}$ | 0.01 1.3 | 0.01 1.1 | 0.02 | 0.01 1.1 | 0.02 | 0.01 1.1 |
| droplets | Herrmann et al. (2010) and Bianco et al. (2020) | Mean Max Min | 2.0×10^{-12} 5.3×10^{-12} 3.8×10^{-14} | 0.02 0.01 0.9 | 0.01 0.01 0.8 | 0.02 0.01 1.0 | 0.01 0.01 0.7 | 0.02 0.01 1.0 | 0.01 0.01 0.8 |
| | Arakaki et al. (2013) | Max Min | 2.0×10^{-12} 1.8×10^{-13} | 0.02 0.2 | 0.01 0.2 | 0.02 | 0.01 | 0.02 | 0.01 0.2 |
| Urban deliquescent particles | Herrmann et al. (2010) | Mean Max Min | 4.4×10^{-13} 1.9×10^{-12} 1.4×10^{-16} | 0.1 0.02 248.0 | 0.1 0.02 204.5 | 0.1 0.02 261.1 | 0.1 0.01 202.5 | 0.1 0.02 261.1 | 0.1 0.02 211.1 |
| | Arakaki et al. (2013) | | 8.0×10^{-13} | 0.04 | 0.04 | 0.05 | 0.04 | 0.05 | 0.04 |
| Remote deliquescent particles | Herrmann et al. (2010) | Mean Max Min | 3.0×10^{-12} 8.0×10^{-12} 5.5×10^{-14} | 0.01 0.004 0.6 | 0.01 0.004 0.5 | 0.01 0.005 0.7 | 0.01 0.004 0.5 | 0.01 0.005 0.7 | 0.01 0.004 0.5 |
| | Arakaki et al. (2013) | | 3.6×10^{-12} | 0.01 | 0.01 | 0.01 | 0.01 | 0.01 | 0.01 |
| Maritime deliquescent particles | Herrmann et al. (2010) | Mean Max Min | 1.0×10^{-13} 3.3×10^{-12} 4.6×10^{-15} | 0.3 0.01 7.5 | 0.3 0.01 6.2 | 0.4 0.01 7.9 | 0.3 0.01 6.2 | 0.4 0.01 7.9 | 0.3 0.01 6.4 |
| | Arakaki et al. (2013) | | 4.0×10^{-16} | 86.8 | 71.6 | 91.4 | 70.9 | 91.4 | 73.9 |
| Gas phase | Prinn et al. (2001) | Mean | 1.0×10^{6} | 39.7 ^c | 132.3 ^d | 15.1 ^c | | 56.4 ^c | |
| | Finlayson-Pitts and Pitts (2000) | Midday | 1.0×10^{7} | 4.0 ^c | 13.2 ^d | 1.5 ^c | | 5.6 ^c | |

^a The units of OH concentrations are M and molecule cm⁻³ in the aqueous and gas phases, respectively.

 \sim 13 h to 5.5 d over the two OH concentrations, which is more than 3 times higher than that from the AOPWIN model. The lifetimes of BTs estimated using mean OH concentrations in the gas phase are significantly longer than those estimated using mean OH concentrations in the aqueous phase, although in rare cases where aqueous-phase OH concentrations are on the order of 10^{-16} M, the estimated lifetimes in the aqueous phase can exceed those in the gas phase by several times. It reveals the high reactivity of BTs with OH radicals in the aqueous phase, suggesting that atmospheric aqueous-phase oxidation could be a significantly effective process to transform these contaminants in the atmosphere.

Significant progress has been made in understanding the formation mechanisms of secondary aerosols, but it is still not possible to quantitatively explain the observed secondary aerosols (Johnston and Kerecman, 2019; Li et al., 2017). This implies the existence of missing sources of precursors and/or unknown atmospheric oxidation mechanisms of known precursors (Goldstein and Galbally, 2007; Wang et al., 2013). In this study, the formation of oxidized organic products with both higher and lower molecular weights was confirmed by LC-Orbitrap MS analysis, and a higher molar yield of sulfate was quantified by IC measurement. Based on these results, aqueous-phase oxidation mechanisms of BTs were proposed, in which OH radicals are assumed to initiate attack

^b The two lifetimes in the aqueous phase are calculated by the rate constants at pH 2 and 10 obtained in this study.

^c The lifetimes in the gas phase are calculated based on the rate constants from the Atmospheric Oxidation Program for Microsoft Windows (AOPWIN) model, which are 0.7, 1.8, and 0.5×10^{-11} cm³ molec. ⁻¹ s⁻¹ for reactions of OH with BT, MBT, and CBT, respectively (USEPA, 2012).

d The lifetimes of BT in the gas phase are calculated by the rate constants determined by a relative rate method, which is $(2.1 \pm 0.1) \times 10^{-12}$ cm³ molec. $^{-1}$ s⁻¹ (Karimova et al., 2024).

on the benzothiazole ring, forming radical intermediates that are subjected to radical-radical coupling, fragmentation, and further oxidation. It suggests that aqueous-phase oxidation of BTs has the capacity to contribute to secondary aerosols, including both inorganic and organic components in the atmosphere. The contribution of secondary aerosols generated from BTs is considered non-negligible and can contribute to the fine particulate matter in some regions where concentrations of BTs are comparable to common aromatic compounds. In addition, yellowish solutions that absorb from the vis to UV wavelengths and have unusual fluorescence spectra are observed after the photooxidation of selected BTs, which suggests that aqueous-phase oxidation of BTs might contribute to the mass of the atmospheric brown carbon. The optical properties might be due to formation of high-molecularweight organic products by radical-radical oligomerization, which is consistent with the measurement result of nanoparticles and confirmed by the LC-Orbitrap MS analysis. Aqueous reactions of BTs have the potential to contribute to the fine particulate air pollution and might significantly modify the chemical compositions and optical properties of atmospheric particles in regions influenced by emissions of BTs and further impact the climate and human health. In the future, research should focus on the occurrence and distribution of BTs in atmospheric aqueous phases, with particular emphasis on integrating real-world concentrations of BTs and varying ambient conditions to advance the understanding of their atmospheric chemistry. Future research should also focus on selection of key secondary products from oxidation of BTs in the ambient atmosphere and their toxicological assessments to evaluate the potential impacts of oxidation of BTs on human health.

Data availability. All data are available from the authors upon request by contacting Jianjie Fu (jjfu@rcees.ac.cn).

Supplement. The supplement related to this article is available online at https://doi.org/10.5194/acp-25-13475-2025-supplement.

Author contributions. QZ: conceptualization, data curation, methodology, investigation, software, visualization, writing (original draft preparation), funding acquisition. WZ: methodology, investigation. ST: conceptualization, methodology. KH: visualization, methodology. JieF: methodology. ZY: conceptualization, methodology. YT: investigation. SS: visualization. YM: investigation. XY: investigation. JiaF: writing (review and editing), supervision, resources, project administration, funding acquisition. GJ: supervision.

Competing interests. The contact author has declared that none of the authors has any competing interests.

Disclaimer. Publisher's note: Copernicus Publications remains neutral with regard to jurisdictional claims made in the text, published maps, institutional affiliations, or any other geographical representation in this paper. While Copernicus Publications makes every effort to include appropriate place names, the final responsibility lies with the authors.

Financial support. This research has been supported by the National Natural Science Foundation of China (grant nos. 22406037, 22376044, and 22476006); the Strategic Priority Research Program of the Chinese Academy of Sciences (grant no. XDB0750100); the Chinese Academy of Sciences Project for the Youth Innovation Promotion Association (grant no. 2022022); the Young Scientists in Basic Research (grant no. YSBR-086); the Postdoctoral Science Foundation of Hangzhou, China (grant no. E2BH2B0604); and the Research Funds of Hangzhou Institute for Advanced Study (grant no. 2023HIAS-P005).

Review statement. This paper was edited by Ivan Kourtchev and reviewed by five anonymous referees.

References

Aljawhary, D., Zhao, R., Lee, A. K. Y., Wang, C., and Abbatt, J. P. D.: Kinetics, mechanism, and secondary organic aerosol yield of aqueous phase photo-oxidation of α-pinene oxidation products, J. Phys. Chem. A, 120, 1395–1407, https://doi.org/10.1021/acs.jpca.5b06237, 2016.

Andreozzi, R., Caprio, V., and Marotta, R.: Oxidation of benzothiazole, 2-mercaptobenzothiazole and 2-hydroxybenzothiazole in aqueous solution by means of H₂O₂/UV or photoassisted Fenton systems, J. Chem. Technol. Biot., 76, 196–202, https://doi.org/10.1002/jctb.360, 2001.

Arakaki, T., Anastasio, C., Kuroki, Y., Nakajima, H., Okada, K., Kotani, Y., Handa, D., Azechi, S., Kimura, T., Tsuhako, A., and Miyagi, Y.: A general scavenging rate constant for reaction of hydroxyl radical with organic carbon in atmospheric waters, Environ. Sci. Technol., 47, 8196–8203, https://doi.org/10.1021/es401927b, 2013.

Armada, D., Llompart, M., Celeiro, M., Garcia-Castro, P., Ratola, N., Dagnac, T., and de Boer, J.: Global evaluation of the chemical hazard of recycled tire crumb rubber employed on worldwide synthetic turf football pitches, Sci. Total Environ., 812, 152542, https://doi.org/10.1016/j.scitotenv.2021.152542, 2022.

Atkinson, R.: Kinetics and mechanisms of the gas-phase reactions of the hydroxyl radical with organic compounds under atmospheric conditions, Chem. Rev., 86, 69–201, https://doi.org/10.1021/cr00071a004, 1986.

Atkinson, R. and Arey, J.: Atmospheric degradation of volatile organic compounds, Chem. Rev., 103, 4605–4638, https://doi.org/10.1021/cr0206420, 2003.

Avagyan, R., Luongo, G., Thorsén, G., and Östman, C.: Benzothiazole, benzotriazole, and their derivates in clothing textiles-a potential source of environmental pollutants and human exposure, Environ. Sci. Pollut. R., 22, 5842–5849, https://doi.org/10.1007/s11356-014-3691-0, 2015.

- Bahnmüller, S., Loi, C. H., Linge, K. L., von Gunten, U., and Canonica, S.: Degradation rates of benzotriazoles and benzothiazoles under UV-C irradiation and the advanced oxidation process UV/H₂O₂, Water Res., 74, 143–154, https://doi.org/10.1016/j.watres.2014.12.039, 2015.
- Bao, M., Zhang, Y.-L., Cao, F., Hong, Y., Lin, Y.-C., Yu, M., Jiang, H., Cheng, Z., Xu, R., and Yang, X.: Impact of fossil and non-fossil fuel sources on the molecular compositions of water-soluble humic-like substances in PM_{2.5} at a suburban site of Yangtze River Delta, China, Atmos. Chem. Phys., 23, 8305–8324, https://doi.org/10.5194/acp-23-8305-2023, 2023.
- Bayati, M., Vu, D. C., Vo, P. H., Rogers, E., Park, J., Ho, T. L., Davis, A. N., Gulseven, Z., Carlo, G., Palermo, F., McElroy, J. A., Nagel, S. C., and Lin, C. H.: Health risk assessment of volatile organic compounds at daycare facilities, Indoor Air, 31, 977–988, https://doi.org/10.1111/ina.12801, 2021.
- Bianco, A., Passananti, M., Brigante, M., and Mailhot, G.: Photochemistry of the cloud aqueous phase: A review, Molecules, 25, 423, https://doi.org/10.3390/molecules25020423, 2020.
- Blando, J. D. and Turpin, B. J.: Secondary organic aerosol formation in cloud and fog droplets: a literature evaluation of plausibility, Atmos. Environ., 34, 1623–1632, 2000.
- Borowska, E., Felis, E., and Kalka, J.: Oxidation of benzotriazole and benzothiazole in photochemical processes: Kinetics and formation of transformation products, Chem. Eng. J., 304, 852–863, https://doi.org/10.1016/j.cej.2016.06.123, 2016.
- Buxton, G. V., Greenstock, C. L., Helman, W. P., and Ross, A. B.: Critical review of rate constants for reactions of hydrated electrons, hydrogen atoms and hydroxyl radicals (•OH/•O⁻) in aqueous solution, J. Phys. Chem. Ref. Data, 17, 513–886, https://doi.org/10.1063/1.555805, 1988.
- Cao, S. T., Liu, J. T., Yu, L., Fang, X. J., Xu, S. Q., Li, Y. Y., and Xia, W.: Prenatal exposure to benzotriazoles and benzothiazoles and child neurodevelopment: A longitudinal study, Sci. Total Environ., 865, 161188, https://doi.org/10.1016/j.scitotenv.2022.161188, 2023.
- Chang, J., Men, Z., Sun, L., Wei, N., Jin, J., Wu, L., Wang, T., and Mao, H.: Study on emission characteristic of benzothiazole and its derivatives from vehicles based on the tunnel experiment, Environ. Pollut. Control, 43, 195–205, https://doi.org/10.15985/j.cnki.1001-3865.2021.02.011, 2021 (in Chinese).
- Chang, J. L. and Thompson, J. E.: Characterization of colored products formed during irradiation of aqueous solutions containing H₂O₂ and phenolic compounds, Atmos. Environ., 44, 541–551, https://doi.org/10.1016/j.atmosenv.2009.10.042, 2010.
- Chen, J., Gu, B., LeBoeuf, E. J., Pan, H., and Dai, S.: Spectroscopic characterization of the structural and functional properties of natural organic matter fractions, Chemosphere, 48, 59–68, https://doi.org/10.1016/S0045-6535(02)00041-3, 2002.
- Chen, X. M., Zhou, Y. Q., Hu, C., Xia, W., Xu, S. Q., Cai, Z. W., and Li, Y. Y.: Prenatal exposure to benzotriazoles and benzothiazoles and cord blood mitochondrial DNA copy number: A prospective investigation, Environ. Int., 143, 105920, https://doi.org/10.1016/j.envint.2020.105920, 2020.
- Chhalodia, A. K., Rinkel, J., Konvalinkova, D., Petersen, J., and Dickschat, J. S.: Identification of volatiles from six marine *Celeribacter* strains, Beilstein J. Org. Chem., 17, 420–430, https://doi.org/10.3762/bjoc.17.38, 2021.

- De Wever, H. and Verachtert, H.: Biodegradation and toxicity of benzothiazoles, Water Res., 31, 2673–2684, https://doi.org/10.1016/s0043-1354(97)00138-3, 1997.
- Desyaterik, Y., Sun, Y., Shen, X., Lee, T., Wang, X., Wang, T., and Collett, J. L.: Speciation of "brown" carbon in cloud water impacted by agricultural biomass burning in eastern China, J. Geophys. Res.-Atmos., 118, 7389–7399, https://doi.org/10.1002/jgrd.50561, 2013.
- Dörter, M., Odabasi, M., and Yenisoy-Karakaş, S.: Source apportionment of biogenic and anthropogenic VOCs in Bolu plateau, Sci. Total Environ., 731, 139201, https://doi.org/10.1016/j.scitotenv.2020.139201, 2020.
- Ervens, B.: Modeling the processing of aerosol and trace gases in clouds and fogs, Chem. Rev., 115, 4157–4198, https://doi.org/10.1021/cr5005887, 2015.
- Ferrario, J. B., Deleon, I. R., and Tracy, R. E.: Evidence for toxic anthropogenic chemicals in human thrombogenic coronary plaques, Arch. Environ. Con. Tox., 14, 529–534, https://doi.org/10.1007/bf01055381, 1985.
- Ferrey, M. L., Hamilton, M. C., Backe, W. J., and Anderson, K. E.: Pharmaceuticals and other anthropogenic chemicals in atmospheric particulates and precipitation, Sci. Total Environ., 612, 1488–1497, https://doi.org/10.1016/j.scitotenv.2017.06.201, 2018.
- Finlayson-Pitts, B. J. and Pitts Jr., J. N.: Chemistry of the upper and lower atmosphere: Theory, experiments, and applications, Academic Press, ISBN 012257060X, 2000.
- Franklin, E. B., Alves, M. R., Moore, A. N., Kilgour, D. B., Novak, G. A., Mayer, K., Sauer, J. S., Weber, R. J., Dang, D., Winter, M., Lee, C., Cappa, C. D., Bertram, T. H., Prather, K. A., Grassian, V. H., and Goldstein, A. H.: Atmospheric benzothiazoles in a coastal marine environment, Environ. Sci. Technol., 55, 15705–15714, https://doi.org/10.1021/acs.est.1c04422, 2021.
- Garcia-Gomez, D., Bregy, L., Nussbaumer-Ochsner, Y., Gaisl, T., Kohler, M., and Zenobi, R.: Detection and quantification of benzothiazoles in exhaled breath and exhaled breath condensate by real-time secondary electrospray ionization-high-resolution mass spectrometry and ultra-high performance liquid chromatography, Environ. Sci. Technol., 49, 12519–12524, https://doi.org/10.1021/acs.est.5b03809, 2015.
- George, K. M., Ruthenburg, T. C., Smith, J., Yu, L., Zhang, Q., Anastasio, C., and Dillner, A. M.: FT-IR Quantification of the carbonyl functional group in aqueous-phase secondary organic Aerosol from phenols, Atmos. Environ., 100, 230–237, https://doi.org/10.1016/j.atmosenv.2014.11.011, 2015.
- Goldstein, A. H. and Galbally, I. E.: Known and unexplored organic constituents in the Earth's atmosphere, Environ. Sci. Technol., 41, 1514–1521, https://doi.org/10.1021/es072476p, 2007.
- Herrmann, H.: Kinetics of aqueous phase reactions relevant for atmospheric chemistry, Chem. Rev., 103, 4691–4716, https://doi.org/10.1021/cr020658q, 2003.
- Herrmann, H., Tilgner, A., Barzaghi, P., Majdik, Z., Gligorovski, S., Poulain, L., and Monod, A.: Towards a more detailed description of tropospheric aqueous phase organic chemistry: CAPRAM 3.0, Atmos. Environ., 39, 4351–4363, https://doi.org/10.1016/j.atmosenv.2005.02.016, 2005.
- Herrmann, H., Hoffmann, D., Schaefer, T., Brauer, P., and Tilgner, A.: Tropospheric aqueous-phase free-radical chemistry: Radical sources, spectra, reaction kinetics

- and prediction tools, ChemPhysChem, 11, 3796–3822, https://doi.org/10.1002/cphc.201000533, 2010.
- Herrmann, H., Schaefer, T., Tilgner, A., Styler, S. A., Weller, C., Teich, M., and Otto, T.: Tropospheric aqueous-phase chemistry: kinetics, mechanisms, and its coupling to a changing gas phase, Chem. Rev., 115, 4259–4334, https://doi.org/10.1021/cr500447k, 2015.
- Jiang, F., Song, J., Bauer, J., Gao, L., Vallon, M., Gebhardt, R., Leisner, T., Norra, S., and Saathoff, H.: Chromophores and chemical composition of brown carbon characterized at an urban kerbside by excitation-emission spectroscopy and mass spectrometry, Atmos. Chem. Phys., 22, 14971–14986, https://doi.org/10.5194/acp-22-14971-2022, 2022.
- Johannessen, C., Saini, A., Zhang, X., and Harner, T.: Air monitoring of tire-derived chemicals in global megacities using passive samplers, Environ. Pollut., 314, 120206, https://doi.org/10.1016/j.envpol.2022.120206, 2022.
- Johnston, M. V. and Kerecman, D. E.: Molecular characterization of atmospheric organic aerosol by mass spectrometry, Annu. Rev. Anal. Chem., 12, 247–274, https://doi.org/10.1146/annurev-anchem-061516-045135, 2019.
- Karimova, N. V., Wang, W., Gerber, R. B., and Finlayson-Pitts, B. J.: Experimental and theoretical investigation of benzothiazole oxidation by OH in air and the role of O₂, Environ. Sci.-Proc. Imp., 26, 2177–2188, https://doi.org/10.1039/D4EM00461B, 2024.
- Kramp, F. and Paulson, S. E.: On the uncertainties in the rate coefficients for OH reactions with hydrocarbons, and the rate coefficients of the 1,3,5-trimethylbenzene and m-xylene reactions with OH radicals in the gas phase, J. Phys. Chem. A, 102, 2685-2690, https://doi.org/10.1021/jp9732890, 1998.
- Lai, W. W.-P., Lin, J.-C., and Li, M.-H.: Degradation of benzothiazole by the UV/persulfate process: Degradation kinetics, mechanism and toxicity, J. Photoch. Photobio. A, 436, 114355, https://doi.org/10.1016/j.jphotochem.2022.114355, 2023.
- Laskin, A., Laskin, J., and Nizkorodov, S. A.: Chemistry of atmospheric brown carbon, Chem. Rev., 115, 4335–4382, https://doi.org/10.1021/cr5006167, 2015.
- Li, F., Tang, S., Tsona, N. T., and Du, L.: Kinetics and mechanism of OH-induced α-terpineol oxidation in the atmospheric aqueous phase, Atmos. Environ., 237, 117650, https://doi.org/10.1016/j.atmosenv.2020.117650, 2020.
- Li, F., Tsona, N. T., Li, J., and Du, L.: Aqueous-phase oxidation of syringic acid emitted from biomass burning: Formation of light-absorbing compounds, Sci. Total Environ., 765, 144239, https://doi.org/10.1016/j.scitotenv.2020.144239, 2021.
- Li, F., Tang, S., Lv, J., He, A., Wang, Y., Liu, S., Cao, H., Zhao, L., Wang, Y., and Jiang, G.: Molecular-scale investigation on the formation of brown carbon aerosol via iron-phenolic compound reactions in the dark, Environ. Sci. Technol., 57, 11173–11184, https://doi.org/10.1021/acs.est.3c04263, 2023a.
- Li, F., Zhou, S., Du, L., Zhao, J., Hang, J., and Wang, X.: Aqueous-phase chemistry of atmospheric phenolic compounds: A critical review of laboratory studies, Sci. Total Environ., 856, 158895, https://doi.org/10.1016/j.scitotenv.2022.158895, 2023b.
- Li, G., Bei, N., Cao, J., Huang, R., Wu, J., Feng, T., Wang, Y., Liu, S., Zhang, Q., Tie, X., and Molina, L. T.: A possible pathway for rapid growth of sulfate during haze days in China, At-

- mos. Chem. Phys., 17, 3301–3316, https://doi.org/10.5194/acp-17-3301-2017, 2017.
- Li, Y., Zhou, Y., Cai, Z., Li, R., Leng, P., Liu, H., Liu, J., Mahai, G., Li, Y., Xu, S., and Xia, W.: Associations of benzotriazoles and benzothiazoles with estrogens and androgens among pregnant women: A cohort study with repeated measurements, Sci. Total Environ., 838, 155998, https://doi.org/10.1016/j.scitotenv.2022.155998, 2022.
- Liao, C., Kim, U.-J., and Kannan, K.: A review of environmental occurrence, fate, exposure, and toxicity of benzothiazoles, Environ. Sci. Technol., 52, 5007–5026, https://doi.org/10.1021/acs.est.7b05493, 2018.
- Liao, X., Zou, T., Chen, M., Song, Y., Yang, C., Qiu, B., Chen, Z.-F., Tsang, S. Y., Qi, Z., and Cai, Z.: Contamination profiles and health impact of benzothiazole and its derivatives in PM_{2.5} in typical Chinese cities, Sci. Total Environ., 755, 142617, https://doi.org/10.1016/j.scitotenv.2020.142617, 2021.
- Lin, P., Rincon, A. G., Kalberer, M., and Yu, J. Z.: Elemental composition of HULIS in the Pearl River Delta Region, China: Results inferred from positive and negative electrospray high resolution mass spectrometric data, Environ. Sci. Technol., 46, 7454–7462, https://doi.org/10.1021/es300285d, 2012.
- Lv, S., Tian, L., Zhao, S., Jones, K. C., Chen, D., Zhong, G., Li, J., Xu, B., Peng, P. A., and Zhang, G.: Aqueous secondary formation substantially contributes to hydrophilic organophosphate esters in aerosols, Nat. Commun., 16, 4463, https://doi.org/10.1038/s41467-025-59361-6, 2025.
- Luongo, G., Avagyan, R., Hongyu, R., and Ostman, C.: The washout effect during laundry on benzothiazole, benzotriazole, quinoline, and their derivatives in clothing textiles, Environ. Sci. Pollut. R., 23, 2537–2548, https://doi.org/10.1007/s11356-015-5405-7, 2016.
- McNeill, V. F.: Aqueous organic chemistry in the atmosphere: Sources and chemical processing of organic aerosols, Environ. Sci. Technol., 49, 1237–1244, https://doi.org/10.1021/es5043707, 2015.
- Meagher, J. F., Olszyna, K. J., Weatherford, F. P., and Mohnen, V. A.: The availability of H₂O₂ and O₃ for aqueous phase oxidation of SO₂. The question of linearity, Atmos. Environ. A-Gen., 24, 1825–1829, https://doi.org/10.1016/0960-1686(90)90514-N, 1990.
- Mei, S. S., Xia, K., Liu, C. C., Chen, X., Yuan, R., Liu, H., Zhao, C., and Liu, S.: Aqueous-phase processing affects the formation and size distribution of aerosol organic functional groups during heavy pollution, J. Geophys. Res.-Atmos., 130, e2024JD042029, https://doi.org/10.1029/2024jd042029, 2025.
- Messaadia, L., El Dib, G., Lendar, M., Cazaunau, M., Roth, E., Ferhati, A., Mellouki, A., and Chakir, A.: Gas-phase rate coefficients for the reaction of 3-hydroxy-2-butanone and 4-hydroxy-2-butanone with OH and Cl, Atmos. Environ., 77, 951–958, https://doi.org/10.1016/j.atmosenv.2013.06.028, 2013.
- Murphy, K. R., Stedmon, C. A., Graeber, D., and Bro, R.: Fluorescence spectroscopy and multi-way techniques. PARAFAC, Anal. Methods-UK, 5, 6557–6566, https://doi.org/10.1039/c3ay41160e, 2013.
- Neumann, M. and Schliebner, I.: Protecting the sources of our drinking water: The criteria for identifying persistent, mobile and toxic (PMT) substances and very persistent and very mobile (vPvM) substances under EU regulation REACH

- (EC) No. 1907/2006, German Environment Agency, ISSN 1862-4804, https://www.umweltbundesamt.de/en/publikationen/protecting-the-sources-of-our-drinking-water-the (last access: 26 August 2025), 2019.
- Nuñez, A., Vallecillos, L., Marcé, R. M., and Borrull, F.: Occurrence and risk assessment of benzothiazole, benzotriazole and benzenesulfonamide derivatives in airborne particulate matter from an industrial area in Spain, Sci. Total Environ., 708, 135065, https://doi.org/10.1016/j.scitotenv.2019.135065, 2020.
- Parker-Jurd, F. N. F., Napper, I. E., Abbott, G. D., Hann, S., and Thompson, R. C.: Quantifying the release of tyre wear particles to the marine environment via multiple pathways, Mar. Pollut. Bull., 172, 112897, https://doi.org/10.1016/j.marpolbul.2021.112897, 2021.
- Prinn, R. G., Huang, J., Weiss, R. F., Cunnold, D. M., Fraser, P. J., Simmonds, P. G., McCulloch, A., Harth, C., Salameh, P., O'Doherty, S., Wang, R. H. J., Porter, L., and Miller, B. R.: Evidence for substantial variations of atmospheric hydroxyl radicals in the past two decades, Science, 292, 1882–1888, https://doi.org/10.1126/science.1058673, 2001.
- Reddy, C. M. and Quinn, J. G.: Environmental chemistry of benzothiazoles derived from rubber, Environ. Sci. Technol., 31, 2847–2853, https://doi.org/10.1021/es9700780, 1997.
- Saini, A., Harner, T., Chinnadhurai, S., Schuster, J. K., Yates, A., Sweetman, A., Aristizabal-Zuluaga, B. H., Jimenez, B., Manzano, C. A., Gaga, E. O., Stevenson, G., Falandysz, J., Ma, J., Miglioranza, K. S. B., Kannan, K., Tominaga, M., Jariyasopit, N., Rojas, N. Y., Amador-Munoz, O., Sinha, R., Alani, R., Suresh, R., Nishino, T., and Shoeib, T.: GAPS-megacities: A new global platform for investigating persistent organic pollutants and chemicals of emerging concern in urban air, Environ. Pollut., 267, 115416, https://doi.org/10.1016/j.envpol.2020.115416, 2020.
- Santos, G. T. A. D., Santos, P. S. M., and Duarte, A. C.: Vanillic and syringic acids from biomass burning: Behaviour during Fenton-like oxidation in atmospheric aqueous phase and in the absence of light, J. Hazard. Mater., 313, 201–208, https://doi.org/10.1016/j.jhazmat.2016.04.006, 2016.
- Schneider, K., de Hoogd, M., Madsen, M. P., Haxaire, P., Bierwisch, A., and Kaiser, E.: ERASSTRI European risk assessment study on synthetic turf rubber infill Part 1: Analysis of infill samples, Sci. Total Environ., 718, 137174, https://doi.org/10.1016/j.scitotenv.2020.137174, 2020.
- Stierle, A. A., Cardellina, J. H., and Singleton, F. L.: Benzothiazoles from a putative bacterial symbiont of the marine sponge Tedania ignis, Tetrahedron Lett., 32, 4847–4848, 1991.
- Tang, J., Li, J., Su, T., Han, Y., Mo, Y., Jiang, H., Cui, M., Jiang, B., Chen, Y., Tang, J., Song, J., Peng, P., and Zhang, G.: Molecular compositions and optical properties of dissolved brown carbon in biomass burning, coal combustion, and vehicle emission aerosols illuminated by excitation–emission matrix spectroscopy and Fourier transform ion cyclotron resonance mass spectrometry analysis, Atmos. Chem. Phys., 20, 2513–2532, https://doi.org/10.5194/acp-20-2513-2020, 2020a.
- Tang, N., Zhang, Z., Dong, R., Zhu, H., and Huang, W.: Emission behavior of crumb rubber modified asphalt in the production process, J. Clean. Prod., 340, 130850, https://doi.org/10.1016/j.jclepro.2022.130850, 2022a.

- Tang, S., Li, F., Tsona, N. T., Lu, C., Wang, X., and Du, L.: Aqueous-phase photooxidation of vanillic acid: A potential source of humic-like substances (HULIS), ACS Earth Space Chem., 4, 862–872, https://doi.org/10.1021/acsearthspacechem.0c00070, 2020b.
- Tang, S., Li, F., Lv, J., Liu, L., Wu, G., Wang, Y., Yu, W., Wang, Y., and Jiang, G.: Unexpected molecular diversity of brown carbon formed by Maillard-like reactions in aqueous aerosols, Chem. Sci., 13, 8401–8411, https://doi.org/10.1039/d2sc02857c, 2022b.
- Teich, M., van Pinxteren, D., Wang, M., Kecorius, S., Wang, Z., Müller, T., Močnik, G., and Herrmann, H.: Contributions of nitrated aromatic compounds to the light absorption of water-soluble and particulate brown carbon in different atmospheric environments in Germany and China, Atmos. Chem. Phys., 17, 1653–1672, https://doi.org/10.5194/acp-17-1653-2017, 2017.
- USEPA: Estimation Programs Interface Suite™ for Microsoft® Windows, v. 4.11, United States Environmental Protection Agency, Washington, DC, USA, https://www.epa.gov/tsca-screening-tools/epi-suitetm-estimation-program-interface (last access: 26 August 2025), 2012.
- Wang, J., Zhou, L., Wang, W., and Ge, M.: Gas-phase reaction of two unsaturated ketones with atomic Cl and O₃: kinetics and products, Phys. Chem. Chem. Phys., 17, 12000–12012, https://doi.org/10.1039/c4cp05461j, 2015.
- Wang, M., Shao, M., Lu, S.-H., Yang, Y.-D., and Chen, W.-T.: Evidence of coal combustion contribution to ambient VOCs during winter in Beijing, Chinese Chem. Lett., 24, 829–832, https://doi.org/10.1016/j.cclet.2013.05.029, 2013.
- Wei, W., Wang, T., Chang, J., and Mao, H.: Emission Characteristics of Benzothiazole and Its Derivatives from Motor Vehicles Based on Tunnel Experiments, China Environ. Sci., 45, 2992–3000, https://doi.org/10.19674/j.cnki.issn1000-6923.20250113.005, 2025 (in Chinese).
- Wishart, D. S., Guo, A., Oler, E., Wang, F., Anjum, A., Peters, H., Dizon, R., Sayeeda, Z., Tian, S., Brian, Berjanskii, M., Mah, R., Yamamoto, M., Jovel, J., Torres-Calzada, C., Hiebert-Giesbrecht, M., Vicki, Varshavi, D., Varshavi, D., Allen, D., Arndt, D., Khetarpal, N., Sivakumaran, A., Harford, K., Sanford, S., Yee, K., Cao, X., Budinski, Z., Liigand, J., Zhang, L., Zheng, J., Mandal, R., Karu, N., Dambrova, M., Helgi, Greiner, R., and Gautam, V.: HMDB 5.0: the Human metabolome database for 2022, Nucleic Acids Res., 50, D622–D631, https://doi.org/10.1093/nar/gkab1062, 2022.
- Wolke, R., Sehili, A. M., Simmel, M., Knoth, O., Tilgner, A., and Herrmann, H.: SPACCIM: A parcel model with detailed microphysics and complex multiphase chemistry, Atmos. Environ., 39, 4375–4388, https://doi.org/10.1016/j.atmosenv.2005.02.038, 2005.
- Wu, Z., Zhu, C., Li, X., Dong, L., Du, B., Wang, W., and Lv, M.: Non-target screening and semi-quantitative analysis of organic pollutants in the atmosphere based on GC-QTOF/MS, Environ. Chem., 40, 3698–3705, https://doi.org/10.7524/j.issn.0254-6108.2021051304, 2021 (in Chinese).
- Yi, Y., Zhou, X., Xue, L., and Wang, W.: Air pollution: formation of brown, lighting-absorbing, secondary organic aerosols by reaction of hydroxyacetone and methylamine, Environ. Chem. Lett., 16, 1083–1088, https://doi.org/10.1007/s10311-018-0727-6, 2018.

- You, B., Li, S., Tsona, N. T., Li, J., Xu, L., Yang, Z., Cheng, S., Chen, Q., George, C., Ge, M., and Du, L.: Environmental processing of short-chain fatty alcohols induced by photosensitized chemistry of brown carbon, ACS Earth Space Chem., 4, 631– 640, https://doi.org/10.1021/acsearthspacechem.0c00023, 2020.
- Zhang, H., Xu, Y., and Jia, L.: A chamber study of catalytic oxidation of SO₂ by Mn²⁺/Fe³⁺ in aerosol water, Atmos. Environ., 245, 118019, https://doi.org/10.1016/j.atmosenv.2020.118019, 2020a.
- Zhang, J., Zhang, X., Wu, L., Wang, T., Zhao, J., Zhang, Y., Men, Z., and Mao, H.: Occurrence of benzothiazole and its derivates in tire wear, road dust, and roadside soil, Chemosphere, 201, 310–317, https://doi.org/10.1016/j.chemosphere.2018.03.007, 2018a.
- Zhang, J., Wang, T., Men, Z., Mao, H., and Wu, Y.: Pollution characteristics and exposure assessment of benzothiazole and its derivatives in ambient air particulates, China Environ. Sci., 40, 851–856, https://doi.org/10.19674/j.cnki.issn1000-6923.2020.0146, 2020b (in Chinese).
- Zhang, L., Li, J., Li, Y., Liu, X., Luo, Z., Shen, G., and Tao, S.: Comparison of water-soluble and water-insoluble organic compositions attributing to different light absorption efficiency between residential coal and biomass burning emissions, Atmos. Chem. Phys., 24, 6323–6337, https://doi.org/10.5194/acp-24-6323-2024, 2024.

- Zhang, Q., Zhang, H., Yu, Z., Fu, J., and Jiang, G.: Occurrence and environmental behavior of benzothiazoles in the atmosphere, Environ. Chem., 44, 1710–1718, https://doi.org/10.7524/j.issn.0254-6108.2024011504, 2025 (in Chinese).
- Zhang, R., Sun, X., Shi, A., Huang, Y., Yan, J., Nie, T., Yan, X., and Li, X.: Secondary inorganic aerosols formation during haze episodes at an urban site in Beijing, China, Atmos. Environ., 177, 275–282, https://doi.org/10.1016/j.atmosenv.2017.12.031, 2018b.
- Zhang, Y., Xu, C., Zhang, W., Qi, Z., Song, Y., Zhu, L., Dong, C., Chen, J., and Cai, Z.: p-Phenylenediamine antioxidants in PM_{2.5}: The underestimated urban air pollutants, Environ. Sci. Technol., 56, 6914–6921, https://doi.org/10.1021/acs.est.1c04500, 2022.
- Zhou, L., Xie, Y., Cao, H., Guo, Z., Wen, J., and Shi, Y.: Enhanced removal of benzothiazole in persulfate promoted wet air oxidation via degradation and synchronous polymerization, Chem. Eng. J., 370, 208–217, https://doi.org/10.1016/j.cej.2019.03.201, 2019
- Zhou, Y. Q., Li, Y., Xu, S. Q., Liao, J. Q., Zhang, H. N., Li, J. F., Hong, Y. J., Xia, W., and Cai, Z. W.: Prenatal exposure to benzotraizoles and benzothiazoles in relation to fetal and birth size: A longitudinal study, J. Hazard. Mater., 398, 122828, https://doi.org/10.1016/j.jhazmat.2020.122828, 2020.